This article was downloaded by:[University of Maryland]
[University of Maryland]
On: 17 July 2007
Access Details: [subscription number 772450216]
Publisher: Taylor & Francis
Informa Ltd Registered in England and Wales Registered Number: 1072954
Registered office: Mortimer House, 37-41 Mortimer Street, London W1T 3JH, UK

Aerosol Science and Technology
Publication details, including instructions for authors and subscription information:
http://www.informaworld.com/smpp/title~content=t713656376

Understanding the Interaction of an Intense Laser Pulse with Nanoparticles: Application to the Quantification of Single Particle Mass Spectrometry

L. Zhou [a]; K. Park [a]; H. M. Milchberg [a]
[a] University of Maryland. College Park, Maryland. USA

First Published on: 01 September 2007
To cite this Article: Zhou, L., Park, K., Milchberg, H. M. and Zachariah, M. R. , (2007) 'Understanding the Interaction of an Intense Laser Pulse with Nanoparticles: Application to the Quantification of Single Particle Mass Spectrometry', Aerosol Science and Technology, 41:9, 818 - 827
To link to this article: DOI: 10.1080/02786820701484955
URL: http://dx.doi.org/10.1080/02786820701484955

PLEASE SCROLL DOWN FOR ARTICLE

Full terms and conditions of use: http://www.informaworld.com/terms-and-conditions-of-access.pdf

This article maybe used for research, teaching and private study purposes. Any substantial or systematic reproduction, re-distribution, re-selling, loan or sub-licensing, systematic supply or distribution in any form to anyone is expressly forbidden.

The publisher does not give any warranty express or implied or make any representation that the contents will be complete or accurate or up to date. The accuracy of any instructions, formulae and drug doses should be independently verified with primary sources. The publisher shall not be liable for any loss, actions, claims, proceedings, demand or costs or damages whatsoever or howsoever caused arising directly or indirectly in connection with or arising out of the use of this material.

© Taylor and Francis 2007

Aerosol Science and Technology, 41:818–827, 2007
Copyright © American Association for Aerosol Research
ISSN: 0278-6826 print / 1521-7388 online
DOI: 10.1080/02786820701484955

Downloaded By: [University of Maryland] At: 16:40 17 July 2007

Understanding the Interaction of an Intense Laser Pulse with Nanoparticles: Application to the Quantification of Single Particle Mass Spectrometry

L. Zhou, K. Park, H. M. Milchberg, and M. R. Zachariah
University of Maryland, College Park, Maryland, USA

Understanding the characteristic behavior of ions produced from the interaction of a high energy laser pulse with nanoparticles is essential for quantitative determination of composition and size of nanoparticles from single particle mass spectrometry (SPMS). We employed a one-dimensional hydrodynamic model, where the laser field is coupled to the non-equilibrium time-dependent plasma hydrodynamics of the heated particles. We focus on regimes of laser width from 0.01 ns to 10 ns (532 nm wavelength, 100 mJ/pulse) and particle size (20–400 nm in diameter) most relevant to commonly used SPMS, and determine the properties of ions generated during the interaction with a strong laser pulse. We compare the simulation results with experiments conducted on aluminum nanoparticles.

The laser-particle interaction is separated into a "soft heating" regime followed by a hydrodynamic expansion. Simulation results showed that the ablation/ionization is effectively complete well before the laser ever reaches its peak intensity. As the pulse width decreased for a given pulse energy, the kinetic energy of ions increased, suggesting that too short a pulse laser (i.e., high laser intensity) would be undesirable because higher energetic ions lead to lower detection efficiency in the SPMS. Results also show that for particle sizes in the range of 100 nm $\sim$ 400 nm, as particle size increased, the kinetic energy of ions produced from the particle increased with a power law relationship, consistent with experiment. Lastly our simulations indicated that ions from the surface of the particle are of higher energy, and therefore have lower detection efficiency.

INTRODUCTION

Many advances in single-particle mass spectrometry for quantitative characterization of size and composition of particles have been made in the last decade (Salt et al. 1996; Suess and Prather 1999; Jayne et al. 2000; Murray 2000; Noble and Prather 2000; Reents and Ge 2000; Kane et al. 2001; Mahadevan et al. 2002). Typically for these experiments a pulsed laser is used as the ionization source, from which time-of-flight mass-spectrometry can be used to deduce composition. The common practice is to use some other method such as light scattering to deduce the size of the particle just prior to ionization, thereby obtaining a measure of both size and composition (Salt et al. 1996). While the technique has proven itself to be highly reliable, it suffers from the limitations inherent to all light scattering, namely the high power dependence on particle size, which has generally limited the technique to particles greater than $\sim$200 nm. More generically a light scattering, or other particle selection approach however, (e.g., mobility selection, size selective aerodynamic focusing) does not take advantage of the inherent capability of the mass spectrometer, to not only provide composition information, but total mass as has been attempted by our group and the work of Reents (Reents and Ge 2000; Lee et al. 2005).

Recently, we and others, with the use of a highly focused pulse laser, determined both total particle mass (i.e., size) and composition quantitatively using only the ion signal from a laser ionization time-of-flight mass spectrometer (Reents and Ge 2000; Mahadevan et al. 2002; Lee et al. 2005; Park et al. 2005). The quantification of composition and size of nanoparticles can be achieved with reasonable accuracy when two primary conditions are met. One is near complete atomization/ionization of the particle constituents (i.e., all neutral atoms are converted to ions with few molecular species), and two, ions produced from the particle should be detected independent of composition and size, or with a known relationship (Lee et al. 2005). Typically a strong laser peak fluence ($\sim 10^{11}$ W/cm^2) that is several orders of magnitude higher than the theoretical energy to atomize and singly ionize all atoms in the particle has been employed. On the other hand, the detection efficiency of ions in the single particle mass spectrometry is highly sensitive to their properties (e.g., kinetic energy) and the laser parameters (e.g., pulse width). The strong laser pulses might produce highly energetic ions so that their transmission efficiency to the detector in the aerosol mass spectrometry (usually through the time-of-flight tube) would be degraded (Lee et al. 2005). This suggests if size-dependent or composition-dependent energetic ions are formed, and their relationships are not understood, it will degrade our ability to quantify the composition and size of particles.

Received 7 December 2006; accepted 31 May 2007.
Support for this work comes from the Army Research Office.
Address correspondence to M. R. Zachariah, Department of Mechanical Engineering, University of Maryland, 2125 Martin Hall, College Park, MD 20852, USA. E-mail: mrz@umd.edu

Downloaded By: [University of Maryland] At: 16:40 17 July 2007

The objective of this article is to understand in greater detail the interaction of a laser pulse with a nanoparticle so as to determine the characteristic properties of ions produced from the particle. In the present study, we employed a modified 1-D hydrodynamic model based on prior work of Milchberg et al (2001) to simulate the temporal evolution of ionization state, and energy as a function of particle size of aluminum that was heated and ionized by a nanosecond 532 nm Nd:YAG laser. The effects of the laser pulse width (i.e., laser intensity) on the ion properties produced after laser-particle interaction were also examined. The simulation results are compared to measurements obtained with a well characterized single particle mass spectrometer (SPMS) (Mahadevan et al. 2002; Lee et al. 2005).

MODEL DESCRIPTION

Several models to describe the interaction of clusters with a laser pulse have been developed (Ditmire et al. 1996; Lezius et al. 1998; Milchberg et al. 2001). In the coulomb explosion model, laser-heated electrons can escape the cluster early in the laser-cluster interaction, leading to a charge buildup in the cluster. This charge buildup will lead electrostatic forces to be dominant in the cluster expansion, resulting in a so-called coulomb explosion. On the other hand, in the hydrodynamic model, the plasma dynamics are driven in response to hydrodynamic forces rather than electrostatic forces. Milchberg et al. showed that the hydrodynamic forces dominate electrostatic forces for clusters larger than 5 nm, and a laser peak intensity of $>10^{14}$ W/cm^2. However, for typical single particle mass spectrometry operation the situation is typically more complicated. For a peak intensity $\sim 10^{11}$ W/cm^2, and particles of 20–400 nm, a purely hydrodynamic model is only valid after sufficient laser heating has taken place to overcome the cohesive energy of the solid. Essentially we can think of the laser interaction process as taking place in two steps. First a rapid laser heating, with evaporation of neutrals from the particle surface followed by a second step of resonant absorption and hydrodynamic plasma expansion.

In a previous work (Rai 2006), we developed a phenomenological model to study the mass and energy transfer processes for the combustion of aluminum nanoparticles. In this study, a similar model was employed to account for the laser-particle heating, and particle evaporative cooling, and integrated into a one-dimensional hydrodynamic model to derive ion properties resulting from a laser-particle interaction (Milchberg et al. 2001). While our calculations are focused on Aluminum, because of our experimental measurements and because modeling a mono-atomic particle are considerably easier, the results on the features of laser-particle interactions are expected to be qualitatively generic, and should lead to a greater mechanistic understanding, and as a guide for future experimental developments.

1. "Soft" Particle Heating

During the early stages of the laser pulse, the laser intensity is relatively low, such that the amount of energy absorbed is below the cohesive energy, so that the particle experiences a "soft" heating and results in neutrals being evaporated. The particle temperature and radius are determined by a coupling of laser heating and evaporative cooling. The effect of vaporization was examined by solving the energy balance in the free molecule regime (Milchberg et al. 2001; Rai 2006). The energy absorbed from the laser, q_{abs} , is balanced with the energy used to evaporate aluminum from the particle, q_{evap} and the energy used to heat the particle, as follows.

$$q_{abs} = q_{evap} + \frac{d}{dt}(m_p c_p T_p) \quad [1]$$

$$q_{abs} = \frac{1}{2}\omega \mathrm{Im}(\gamma)\,|E|^2 \quad [2]$$

$$q_{evap} = L_{vap,Al} \times w_{Al} \times 4\Pi r^2 \quad [3]$$

Here m_p is the mass of aluminum particle, c_p is the specific heat of aluminum, r is the radius of particle, and T_p is the temperature of particle. q_{abs} can be calculated using laser angular frequency ω, the imaginary part of particle polarizability $\mathrm{Im}(\gamma)$ and the electric field generated by the laser E, $L_{vap,Al}$ is latent heat of vaporization for aluminum, w_{Al} is the free molecular evaporation flux of aluminum atoms, and is given by

$$w_{Al} = \frac{P_d}{\sqrt{2\Pi RTM}} \quad [4]$$

R is the gas constant, and P_d is the equilibrium vapor pressure of aluminum as determined by the Kelvin equation:

$$P_d = P_0 \times \exp\left(\frac{4\sigma v_1}{T(ev)d \times 1.6 \times 10^{-19}}\right) \quad [5]$$

Here P_0 is the vapor pressure over a flat surface at temperature T, σ is the surface tension of aluminum, v_1 is the monomer volume and d is the diameter of the drop. Vapor pressure P_0 and surface tension σ can be calculated by Equations (5) and (6).

$$P_0 = \exp\left(13.07 - \frac{3}{T(ev)}\right) \times 1.01 \times 10^6 \text{ Dyne/cm}^2 \quad [6]$$

And

$$\sigma = 948 - 0.245 \times 10^4 T(ev) \text{ Dyne/cm} \quad [7]$$

The use of Equation (7) is only valid to approximate 0.5 ev, at which point the surface tension becomes negative implying that the particle is mechanically unstable. In such a case, the free molecular evaporation rate w_{Al} is obtained from the effective equilibrium condensation rate and detailed balancing (Friedlander 2000)

$$w_{Al} = \frac{P_0}{\sqrt{2\Pi RTM}} \quad [8]$$

Downloaded By: [University of Maryland] At: 16:40 17 July 2007

The energy balance is solved to obtain a temporal profile of particle size and temperature, and the results are used as input parameters for the hydrodynamic model.

2. Hydrodynamic Model

The hydrodynamic simulation is based on a one-fluid two temperature (i.e., electron and ion temperature) model, which includes thermal conduction, and a collision-radiative model for the ionization dynamics, the complete details for which are presented elsewhere (Milchberg et al. 2001). Briefly, the laser's electric field (= E(r), 1-D solid angle averaged electric field) is used to heat, and ionize the particle, and to advance the non-equilibrium time-dependent plasma hydrodynamics of the heated particle. The electric near field is described by, $\nabla \cdot (\varepsilon \mathrm{E}) = 0$, where $\varepsilon(\mathrm{r})$ is the dielectric function, and is coupled to a 1-D radial Lagrangian hydrocode. A near field approximation is appropriate for the case when the product, ka $\ll 1$, where k $(= 2\pi/\lambda)$ is the laser wave number, and a is the particle radius. For example, for a 20 nm diameter particle, excited with a visible laser, ka$\sim$0.1. The dielectric response ($\varepsilon(\mathrm{r})$) of the laser-heated plasma is taken to be a Drude form, which is appropriate for strongly heated near-solid-density plasmas with little electronic band structure (Parra et al. 2003). The 1-D radial Lagrangian hydrocode model is outlined below including the mass (9), momentum (10), and energy (11) equations.

$$\frac{\partial \rho}{\partial t} + \nabla \cdot (\rho \vec{v}) = 0 \qquad [9]$$

$$\frac{\partial \rho \vec{v}}{\partial t} + \nabla \cdot (\rho \vec{v}\vec{v} + P) = 0 \qquad [10]$$

$$\frac{\partial(\rho e + \frac{1}{2}\rho v^2)}{\partial t} + \nabla \cdot \left(\left(\rho e + \frac{1}{2}\rho v^2 \right) \vec{v} + P\vec{v} + \vec{q} \right) = S_{laser} \pm S_{\text{ionization / recombination}} \qquad [11]$$

where ρ is the mass density, v is the fluid velocity, P is the pressure, taken to be isotropic, e is the internal energy per unit mass of the fluid, q is the heat flux, S_{laser} is the energy deposition rate by the laser per unit volume, and $S_{\text{ionization/recombination}}$ is the energy stored in the ionization state of the plasma, and the plasma internal energy. The rate equation for the ion species, which includes collisional ionization, recombination, and field ionization, are as follows:

$$\frac{dN_j}{dt} = S_{j-1}N_{j-1}N_e - (S_j + \alpha_j)N_jN_e + (\alpha_{j+1})N_{j+1}N_e + w_{j-1}(|E|)N_{j-1} - w_j(|E|)N_j \qquad [12]$$

where N_j is the number density of ion at the ionization state j, S_j is the collisional ionization rate, α_j is the recombination rate, N_e is the electron density, E is the laser electric field, and w_j is the field ionization coefficient (Ammosov et al. 1986). At each time step, the electric near field is solved using the density and temperature profiles of neutrals, ions, and electrons of the previous time step. The resulting electric field ionizes, and heats the plasma, temporally evolving the density and temperature profiles. Field and collisional ionization, recombination, and thermal conduction either gradient based or flux limited are taken into account in the calculation as shown in the above equations. The ideal gas equation of state is used to relate the plasma temperature and pressure.

SINGLE PARTICLE MASS SPECTROMETER

In order to experimentally determine the relationship between particle size and the amount of ions detected with the single particle mass spectrometer (SPMS), we first need to generate aerosols and transport them to the SPMS. For generation of aerosols, we dispersed commercial aluminum nanopowders (Aveka Inc.) in methanol, and silver nitrate and sodium chloride in deionized water, and suspended them in the air using a Collison atomizer. These particles were passed through several aerosol diffusion driers to remove the solvent. The aerosol was then passed through a differential mobility analyzer (DMA) (Knutson and Whitby 1975) to select particles of known size for direct delivery to the inlet of the SPMS. Detailed descriptions on the SPMS can be found in our previous article (Mahadevan et al. 2002; Park et al. 2005). Briefly, the SPMS consists of an aerodynamic lens inlet, three stage differential vacuum systems, a free firing pulsed laser for particle ionization, a linear time-of-flight mass spectrometer, and a 500 MHz digital oscilloscope and PC for data acquisition. The aerodynamic lens system produces a narrow collimated particle beam and transports particles of 30–300 nm into the high vacuum system with a high transmission efficiency. The free firing pulsed laser (a frequency-doubled Nd:YAG laser operated at 10 Hz, 532 nm wavelength), through a spherical plano-convex lens, is tightly focused at the extraction field of the mass spectrometer and intersects the particle beam with a laser beam diameter of $\sim$0.1 mm and a laser pulse duration of $\sim$5 ns. We have found that a pulse energy of $\sim$100 mJ/pulse, corresponding to a peak laser power density at the focal point of approximately $\sim 10^{11}$ W/cm^2, provided sufficiently high level of ion currents to provide quantitative composition measurement. When the laser hits a particle successfully, positive ions formed from the particle are accelerated along $\sim$1 m time-of-flight tube and detected by microchannel plates (MCP).

RESULTS AND DISCUSSION

In our present (experimental) study, aluminum nanoparticles are irradiated with a 532 nm, 5 ns FWHM 100 mJ Gaussian pulse (Nd:Yag laser) with a peak laser intensity of $\sim 1.55 * 10^{11}$ W/cm^2. As mentioned above, the particle first undergoes a soft heating process to overcome the cohesive energy of aluminum and then transitions to a hydrodynamic plasma

Downloaded By: [University of Maryland] At: 16:40 17 July 2007

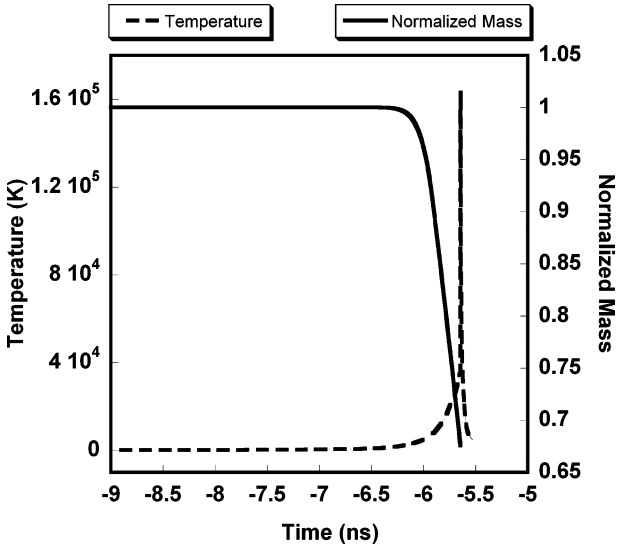

FIG. 1. Simulation of soft laser heating of 100 nm Aluminum as a function to time. Time = 0 corresponds to the peak in the 532 nm, 5 ns FWHM 100 mJ Gaussian laser pulse.

expansion. The temporal and spatial profiles (1-D) for density, temperature, and velocity of electrons and ions from the laser-particle interaction can be obtained by a complete simulation of both models.

Figure 1 shows results for the temporal variation in temperature and particle mass, for the early stage of particle heating for aluminum of 100 nm diameter. The laser peak is at t = 0 and the interaction between laser and particle is observed from t = −9 ns. As discussed above, the cohesive energy of aluminum will delay the hydrodynamic expansion of the particle in the early stage of the laser-particle interaction, until the temperature reaches the cohesive energy threshold (∼3 eV). After the particle temperature reaches the cohesive energy threshold, electrons and ions energies are high enough such that the particle rapidly transitions into a dense plasma and expands in response to hydrodynamic forces, where the high-density collisional processes are dominant in particle ionization and heating. During hydrodynamic expansion, the particle is rapidly heated to a very high temperature ($>10^5$ K) and then cools rapidly due to expansion cooling as shown in Figure 1. It is also interesting to note that the temperature increases so rapidly that particle heating is much faster than the ability to evaporate mass, as evidenced by the very small evaporation loss from the particle during the soft heating.

The normalized electron density and electric field for a 100 nm diameter particle during the hydrodynamic expansion are presented in Figure 2(a) and (b). The initial electron density of aluminum is $6.026 * 10^{22}/\text{cm}^3$. In Figure 2 (a) the electron density (N_e) is normalized by the critical plasma density ($N_{cr} = m_e\omega^2/4\pi e^2 = 3.95 * 10^{21}/\text{cm}^3$) where m_e is the electron mass, ω is the laser frequency, and e is electron charge. Results are presented from the point in time when the temperature

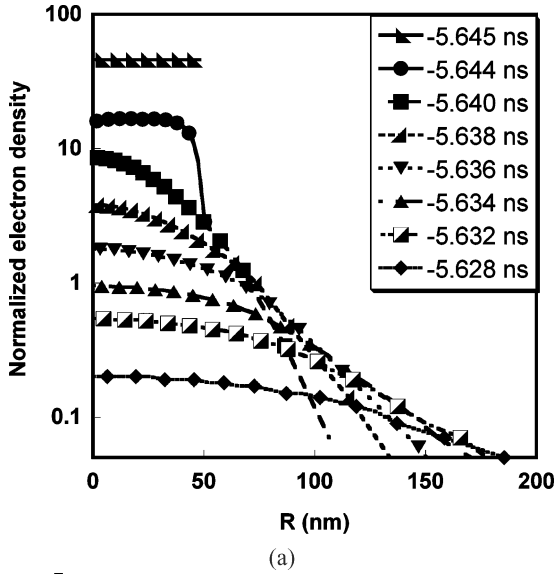

(a)

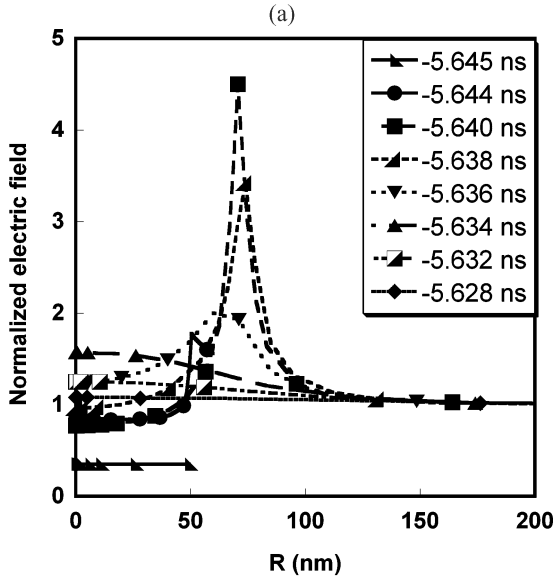

(b)

FIG. 2. (a) Temporal and radial spatial variation of normalized electron density. (b) Temporal and radial spatial variation of the normalized electric field.

reaches the cohesive energy threshold, at −5.644 ns. The critical plasma density defines the point below which the plasma becomes transparent to the laser beam, and no further energy deposition takes place. Figure 2(a) indicates that the electron density profile is non-uniform during the expansion, and that there is a critical density surface (i.e., $N_e \sim N_{cr}$) where resonant laser light absorption occurs, and is maintained from −5.644 ns to −5.634 ns, about ∼10 ps. Figure 2(b) presents the vacuum level normalized electric field during the hydrodynamic expansion as a function of radial location and time. Near the region of the critical density surface (radial location) the corresponding electric field is significantly enhanced with respect to its vacuum value as shown in Figure 2(b). This time (∼10 ps) can be defined as the critical density lifetime (τ_{cr}), which is the time for a

Downloaded By: [University of Maryland] At: 16:40 17 July 2007

laser heated cluster to expand to a local electron density, which is below the critical density (i.e., $N_e < N_{cr}$). At times greater than the critical density lifetime (τ_{cr}), laser light absorption will decrease significantly.

The results from Figure 2(a) and (b) indicates that the laser-particle interaction occurs over a period of ~3 ns (from −9 ns to −5.6 ns) for the Gaussian 5 ns FWHM laser pulse, and that most of the time is spend to overcome the cohesive energy threshold. On the other hand, if we look at the absolute energy deposited to the particle during the interaction (Figure 3), it is clear that although the hydrodynamic plasma expansion occurs over a very short time (~10 ps), the energy deposition rate is much faster (~10^{12} ev/sec) than in the "soft heating" regime (18 eV in 3 ns). Figure 3 also shows that the energy deposition is completed after the critical density life time, which is consistent with the discussion above.

Thus, in our nanosecond laser pulse, the energy absorption of the particle only takes place during the leading edge of the pulse, and after τ_{cr}, the coupling is no better than in a gas. In other words, the ablation/ionization is over well before a nanosecond laser ever reaches its peak intensity. This observation is qualitatively consistent with previous results for the interaction of the laser pulse (peak intensity $>10^{14}$ W/cm^2) with argon clusters (Parra et al. 2003).

As mentioned early, the SPMS can be used to estimate particle size using the predetermined relationship between the ion signal (i.e., the amount of ions detected in the measured mass spectrum) and particle size. However, the formation of energetic ions will affect the transport efficiency through the SPMS time-of-flight tube and therefore sensitivity. In our previous study (Lee et al. 2005), we defined the detection efficiency (DE) as

$$\mathrm{DE} = \frac{\text{number of ions detected by SPMS}}{\text{total number of ions}}$$

the ion trajectories in the TOF tube were simulated using SIMION, and the detection efficiency was calculated as a function of initial ion kinetic energy. The result shown in Figure 4 demonstrates that the detection efficiency for ions in the SPMS depends strongly on the ion-kinetic energy;

$$\mathrm{DE}\ (\%)\ (\text{detection efficiency}) \sim E_k^{-0.99};$$

i.e., as the kinetic energy of ions increase, the detection efficiency decreases.

Clearly, the initial kinetic energy of ions plays an important role in the application of SPMS: ions with high kinetic energy are harder to collimate with the extraction fields and as a consequence, both the detection sensitivity, and the ability of quantitatively characterize single nanoparticle are degraded. Thus we are especially interested in the kinetic energy of constituent ions produced from the laser pulse. The remainder of this article explores the influence of the laser pulse intensity on the kinetic energy of ions produced from the laser-particle interaction, as well as the particle size dependent energetic ion formation.

The kinetic energy of ions was computed using the velocity profiles obtained from the simulation results. Figure 5(a) shows the kinetic energy (=1/2 mv^2) profiles as a function of radial distance at various times, for an aluminum particle of initial diameter of 100 nm. Evidently the ions at the surface of the expanding plasma cloud have the highest kinetic energy. From the practical point of view a bias to higher kinetic energy for the surface atoms will lead to lower detection efficiency as shown in Figure 4 and therefore a bias against surface species. We have

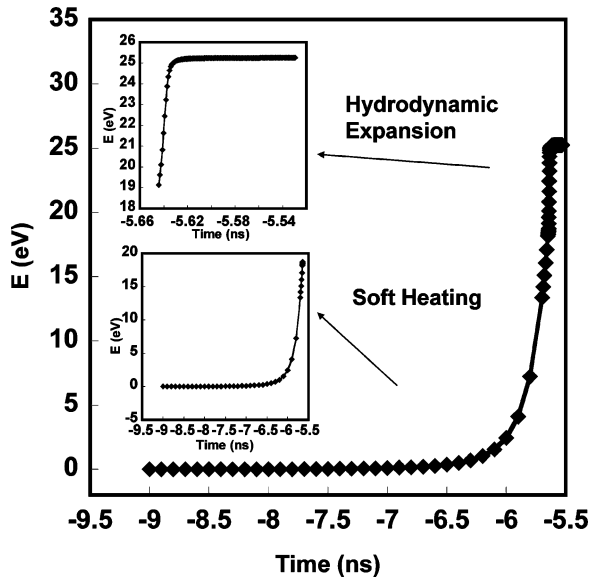

FIG. 3. Total absolute energy deposited to the particle during the laser interaction.

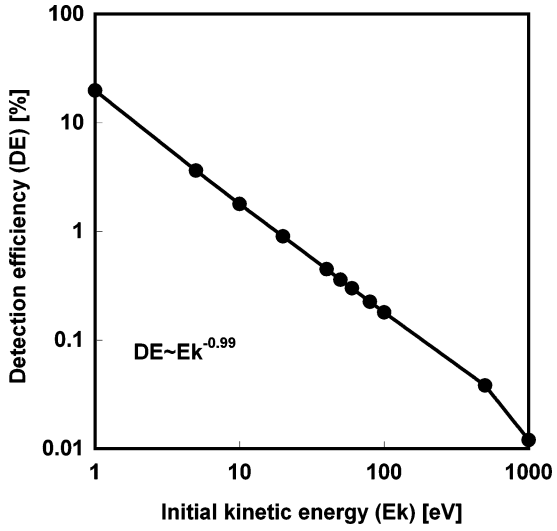

FIG. 4. Calculated effect of initial kinetic energy on detection efficiency of the SPMS.

Downloaded By: [University of Maryland] At: 16:40 17 July 2007

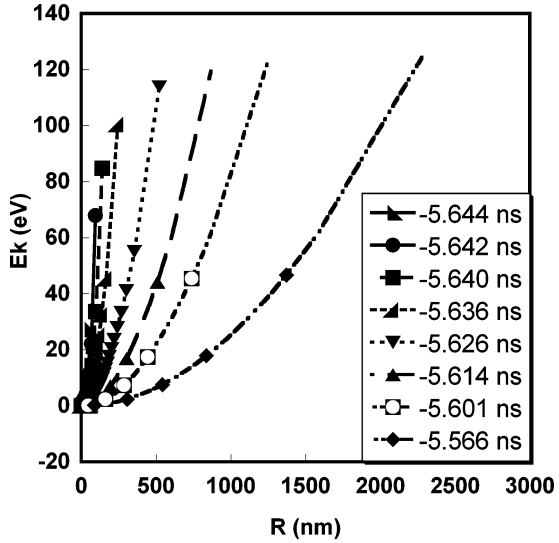

(a)

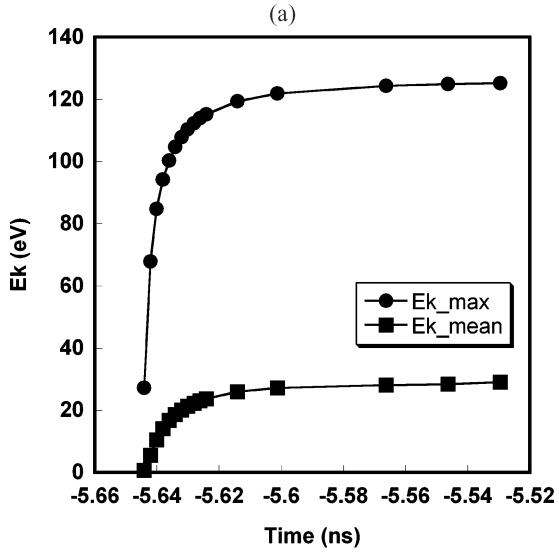

(b)

FIG. 5. (a) Kinetic energy profile as a function of radial distance at various times for an aluminum particle of initial diameter = 100 nm. (b) Temporal variation of the average and maximum kinetic energy for an aluminum particle of initial diameter = 100 nm.

also plotted the number weighted average kinetic energy (i.e., E_k_mean $= \Sigma\ E_k(r) * N_i\ (r)\ /\ \Sigma\ N_i$ where r is the radius and N is the ion number), and its maximum value against time in Figure 5(b). Note that the kinetic energy increases rapidly initially, but reaches an asymptotic value after ~ -5.634 ns. This occurs because most of laser energy is absorbed onto the particle during the leading edge of the pulse till we achieve τ_{cr} ($\sim$10 ps).

The hydrodynamic simulation results suggested that most of the laser energy is not deposited into the particle because of the poor coupling between laser pulse and the plasma. Obviously, for the single particle mass spectrometer, a hot plasma is preferable to ensure complete ionization, which can be achieved by employing a higher laser intensity or absorption efficiency. However, a hotter plasma should produce more energetic ions, which will result in greater ion loss during the transport in the TOF. In other words, too intense a photon flux or too much absorption may decrease the overall ability to quantify SPMS data, by possible species biases in the detection efficiency of ions, while too weak a laser cannot ensure complete conversion of constituent atoms to ions. Ideally one would like to understand where the optimum lies.

Based on the above discussion, we conducted simulations to investigate ion formation from a 100 nm aluminum nanoparticle after their interaction with laser light of varying pulse widths (10 ps $\sim$ 10 ns). The motivations are based on our previous discussion that indicated that the critical plasma density is achieved well before a nanosecond laser reaches its peak intensity. Furthermore all experimental work on particle mass spectrometry to date, at least to our knowledge has employed nanosecond lasers. To explore the role of pulse width we used the following conditions for our simulation; 10 ps (7.75×10^{13} W/cm^2), 100 ps (7.75×10^{12} W/cm^2), 0.5 ns (1.55×10^{12} W/cm^2), 5 ns (1.55×10^{11} W/cm^2), 10 ns ($=7.75 \times 10^{10}$ W/cm^2), Figure 6 plots the number weighted average kinetic energy and average ionization state of ions for different laser intensity. The results show a monotonic increase in both the mean kinetic energy and average charge of ions as the pulse width is decreased. The results indicate that going to a shorter laser pulse creates a much more aggressive laser interaction. If we consider the nano-second laser sources as our base case condition, it is quite clear that a longer pulse laser would be the wrong direction to go to ensure the complete ionization approach. The next question is if pico-second lasers which are readily available offer some advantages. The results suggested that for a pico-second laser, the mean kinetic energy and average ionization state of ions could be very high, such that complete ionization criterion can be guaranteed, however, the higher kinetic energy of ions will

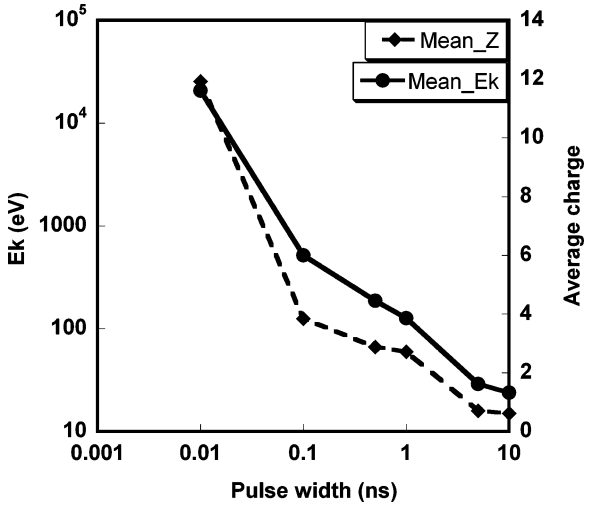

FIG. 6. Effect of laser pulse width on average kinetic energy and average ionization state for an aluminum particle of initial diameter = 100 nm.

Downloaded By: [University of Maryland] At: 16:40 17 July 2007

result in a low detection efficiency given standard ion optics employed in TOF systems. On the other hand the pico-second laser has the highest likelihood that poor absorbers of surface coated material that might preferentially be blown-off without being ionized may be detected with a shorter pulse laser providing a more aggressive ionization (Zhou et al. 2006).

The above result invites the question, would a lower pulse energy for pico-second lasers have some advantages for SPMS application. Further simulations for 100 ps and 10 ps pulses were carried out with laser pulse energy of 50 mJ and 10 mJ. As one would expect, the simulations give lower mean ion kinetic energy and average charge of ions with the decrease of laser pulse energy, but in general is seen to be a an insensitive parameter, likely because the absorption time is shorted than the pulse duration in any case. Thus once a threshold energy is achieved the resulting ionization process becomes relatively insensitive to pulse energy. For example, as the laser pulse energy decreases from 100 mJ to 10 mJ, the resulting ions mean kinetic energy decreases by a factor of 1.3 (from 517 eV to 395 eV), and 1.04 (from 20762 eV to 19826 eV) for 100 ps and 10 ps lasers, respectively. This also implies that a pico-second laser with near threshold energy would provide enough ionization with low ion kinetic energy. Simulations on a 10 ps pulse with lower pulse energy show that the threshold energy is on the order of hundreds of microjoules. So a 1 mJ pulse would give a kinetic energy of 18186 eV while the resulting ions mean kinetic energy of a 0.5 mJ pulse is only 226 eV and the interaction takes place over the whole laser pulse. Further decrease of the pulse energy to 0.1 mJ, results in insufficient energy absorbed to overcome the cohesive energy threshold, and as a result no hydrodynamic plasma formation.

The present results suggest that a nano-second laser may in fact provide the optimal laser source, for the present design of time-of-flight optics. However, experiments on pico-second laser are warranted. In the latter case, other configurations, such as a high pressure ionization region where the kinetic energy of ions can be absorbed may offer interesting avenues for exploiting pico-second lasers (Wang et al. 2006).

To further illustrate the effect of laser pulse width on the laser-particle interaction, the normalized Gaussian laser pulses are plotted in Figure 7(a). For each laser pulse, we also define the temporal regions that correspond to the "soft heating" and hydrodynamic expansion, and the fraction of laser energy absorbed as a function of pulse width plotted in Figure 7(b). Note that in Figure 7(a), we should compare the relative fraction of "soft heating" and hydrodynamic expansion time in each pulse rather than the absolute interaction time. We can see that the hydrodynamic interaction regime become significantly longer as the laser pulse width is decreased. Considering that the energy absorption during this part of the interaction is much more aggressive, the result shown in Figure 7(a), implies that there is more energy deposited onto the particle for a shorter laser pulse, which is manifested as an increase in ion energy and ionization state. This conclusion is confirmed by the calculation of energy absorption efficiency shown in Figure 7(b), which indicates a monotonic increase in absorption efficiency as the pulse width is decreased.

Next we turn our attention to the effect of particle size on the kinetic energy of ions produced. In our previous work, we hypothesized that the non-linear relationship between the ion signal and particle size observed in our experiment is due to the formation of size-dependent energetic ions (Lee et al. 2005). In this work, simulations of laser interactions with particles in size range of 20∼400 nm were carried out and the resulting ions energy were examined to understand their size dependence.

The number weighted average kinetic energy for particles in the 20–400 nm range are shown in Figure 8. We found that as size increases, the average kinetic energy of ions increases, and for particle size ∼100 nm and larger, the kinetic energy follows a power law relationship in particle diameter ($E_k \sim D_p^{1.43}$). One possible explanation for the size-dependent kinetic energy formation is that with increasing particle size, the critical density lifetime increases (i.e., it takes longer for the average density of the larger particle to drop below the critical density), and therefore the particle absorbs energy for a longer period of time. Increased absorption time results in greater heating, leading to a higher initial kinetic energy and charge state for larger particles.

We are now in a position to compare the simulation results with our experiment. In our previous study (Lee et al. 2005), we simulated the detection efficiency (DE) of ions traveling through the time-of-flight tube in the single particle mass spectrometry, and showed that the DE depends on their initial kinetic energy (E_k), providing the relationship DE (%) $\sim E_k^{-0.99}$. This indicates that DE decreases with higher kinetic energy ions. In that study, we hypothesized that the non-linear relationship between ion peak area, and particle size was caused by the more energetic ion formation from larger particles. Our current simulation results ($E_k \sim D_p^{1.42}$) qualitatively showed that this should be true.

By employing the relationship ($E_k \sim D_p^{1.43}$) from the current simulation results, and the DE (%) $\sim E_k^{-0.99}$ from the previous ion trajectory simulation, we obtain DE (%) $\sim D_p^{-1.42}$. Since the DE is related to the integrated peak area in a single particle mass spectrum by the equation of

$$\text{Peak Area} = \text{C} \times \text{DE} \times \text{total number of ions}$$

where C is the proportionality constant between detector signal (peak area) and the number of detected ions. Thus, we can obtained the relationship between the integrated peak area and particle size, giving peak area $\sim D_p^{1.58}$, or peak area$^{1/3} \sim D_p^{0.53}$, and the proportionality constant C can also be determined by fitting the above relation to the experimental data of aluminum. Now we compare the above relationship (peak area$^{1/3} \sim D_p^{0.53}$) with experimental measurements with the single particle mass spectrometer for aluminum particles. The comparisons shown in Figure 9 clearly indicate that the simulation correctly captures the basic trends observed in the experiment. The power

Downloaded By: [University of Maryland] At: 16:40 17 July 2007

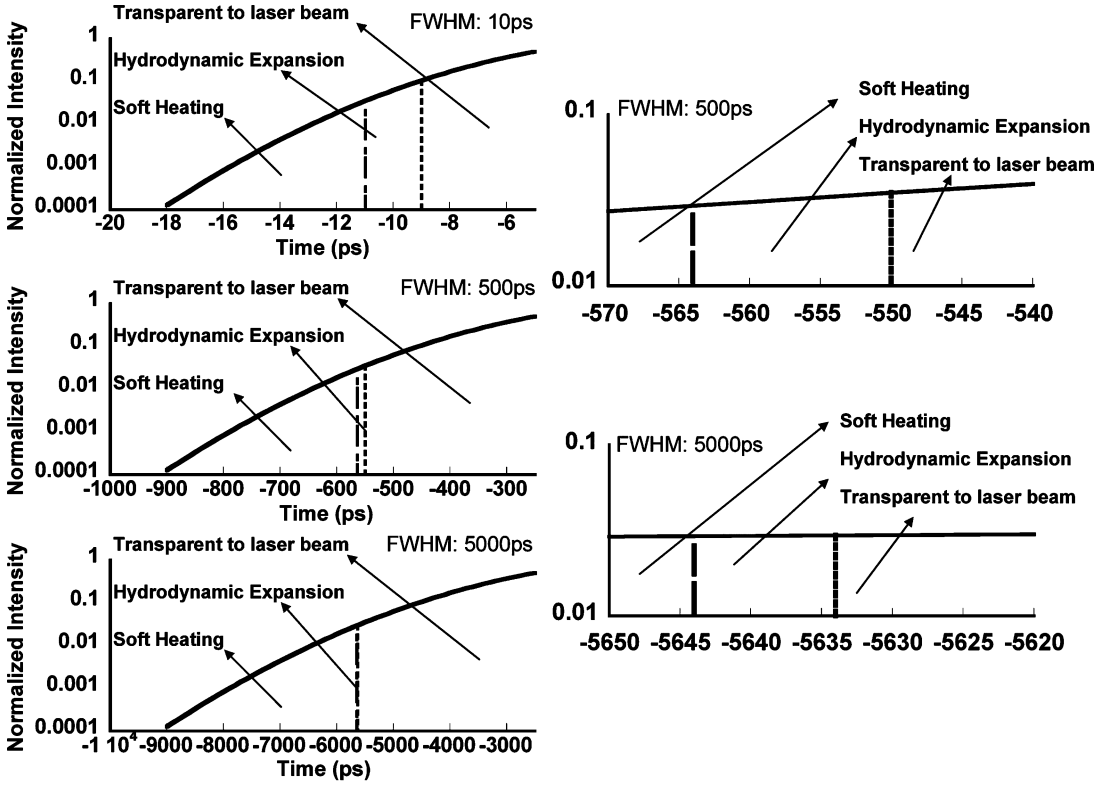

(a)

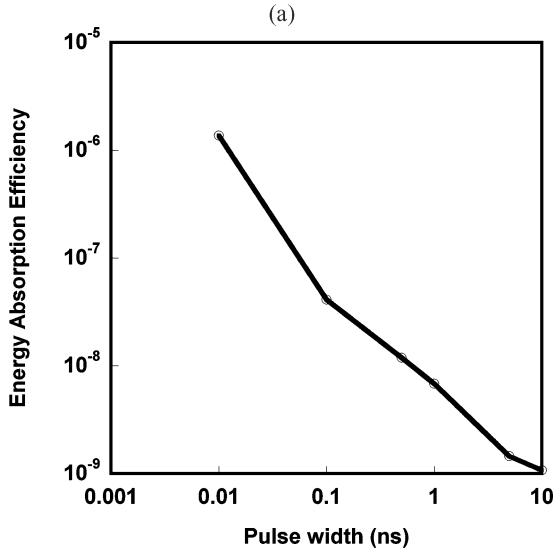

(b)

FIG. 7. (a) Left: Gaussian laser pulses of various width overlayed with the "soft-heating" and hydrodynamic expansion regions for an aluminum particle of initial diameter = 100 nm. Right: Detailed view of "soft-heating" and hydrodynamic expansion regions for FWHM 5000 ps and FWHM 500 ps laser pulses. (b) Calculated fraction of laser energy absorbed in a 100 nm aluminum particle as a function of pulse width.

dependence from the theoretical calculations for aluminum particles is 0.53, while the experimental values are 0.58. The experimental results for a variety of materials are also shown in Figure 9. The power dependence between peak area$^{1/3}$ and particle size is 0.45, 0.30, for sodium chloride and silver nitrate, respectively. Based on the data presented in Figure 9 it is quite reasonable to assume the proportionality constant C between signal and number of ions detected is material independent, so that with the value obtained for aluminum, we can estimate the KE of other materials. Our estimate yields a value for mean KE of about 5.13 eV and 19.3 eV for ions generated from a 100 nm sodium chloride and silver nitrate particle, respectively.

Downloaded By: [University of Maryland] At: 16:40 17 July 2007

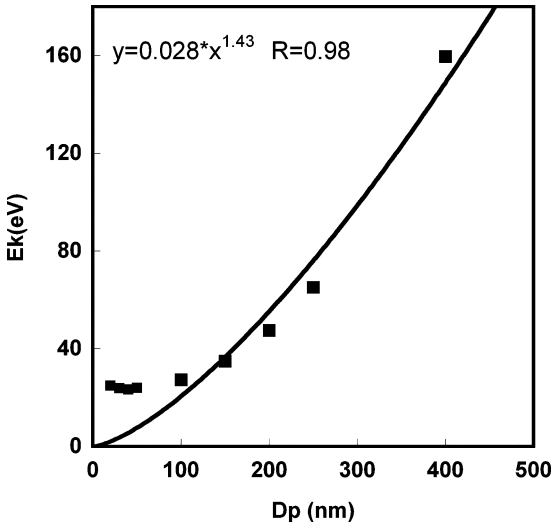

FIG. 8. Mean kinetic energy of ions as a function of particle diameter.

Compared to the with mean KE of 29 eV for 100 nm aluminum, our experimental results suggest that even though particles of different materials would have different KEs, the MS signal are remarkably similar. This should be expected because the experimental result is mass based (peak area corresponding to mass of particle), which is $\sim Dp^3$. So the peak area obtained from experiment is less sensitive to Dp, and hence not as sensitive to KE. In fact, this is one of the potential advantages of using SPMS to determine particle size: with a pre-determined power dependence, we can quantitatively determine particle size within a reasonable accuracy regardless of particle composition.

It is also interesting to note that for smaller particles, there is a discrepancy between the average kinetic energy and the power law relationship, $E_k \sim D_p^{1.43}$, obtained above, the kinetic energy for particles in small size range have a relative higher value. The high kinetic energy suggests a relatively more aggressive energy absorption and particle ionization for a smaller particle. This result is consistent with a recent experimental observation by Wang et al. (2006) who developed a nanoaerosol mass spectrometer (NAMS) using the complete ionization technique. Quantitative chemical characterization for a particle with diameter $\sim$10 nm was achieved with a quadrupole ion guide and quadrupole ion trap system. In their work, multiple charged ions peaks (+4) were frequently observed in the spectra, which imply highly ionization states were achieved for particle sizes $<\sim$10 nm.

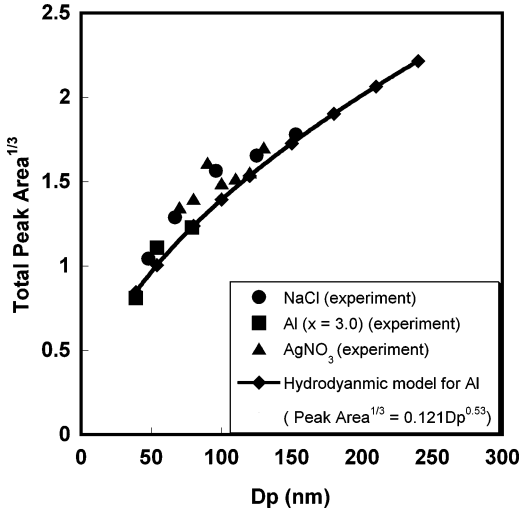

FIG. 9. Comparison of the relationship between ion peak area and particle size from simulation results, and experimentally determined by the single particle mass spectrometer.

CONCLUSIONS

The objective of this article was to understand pulsed laser interactions with small particles as it applies to the implementation and quantification of single particle mass spectrometry. In this study we applied a one-dimensional hydrodynamic model to determine the characteristic behavior of ions produced from aluminum nanoparticles as a result of interaction with a strong laser pulse. During the early stages of interaction, the particle experiences a "soft heating" regime to overcome the cohesive energy of solid. Subsequently, the laser–particle interaction transitions to a resonant absorption and hydrodynamic plasma expansion. The effect of laser parameters such as pulse width, energy, and particle size were investigated in this work.

Our simulation results showed that the ablation/ionization process is finished well before the laser ever reaches its peak intensity. We found that shorter laser pulses lead to greater energy absorption and produce a more intense plasma, which will result in higher ionization state and higher ion kinetic energy. However the higher kinetic energy of the shorter pulse lasers will likely lead to a significantly degraded detection efficiency for ions in traditional TOF ion optics. The simulations suggested that nano-second lasers may, in fact, provide an optimized solution for SPMS application.

We also found particle size-dependent energetic ions are formed from the laser-particle interaction, and the kinetic energy of ions is proportional to the particle size with a power law relationship ($E_k \sim D_p^{1.42}$). This result is show to be consistent with our experimental observation, and suggest that particle size-dependent energetic ions led to the power-law relationship between peak area and particle size observed in a single particle mass spectrometer.

REFERENCES

Ammosov, M. V., Delone, N. B., and Kraînov, V. P. (1986). Tunnel Ionization of Complex Atoms and Atomic Ions in a Varying Electromagnetic-Field, *Zhurnal Eksperimentalnoi I Teoreticheskoi Fiziki* 91(6): 2008–2013.

Ditmire, T., Donnelly, T., Rubenchik, A. M., Falcone, R. W., and Perry, M. D. (1996). Interaction of Intense Laser Pulses with Atomic Clusters, *Physical Review A: Atomic, Molecular, and Optical Physics* 53(5): 3379–3402.

Friedlander, S. F. (2000). *Smoke, Dust, and Haze*. Oxford University Press, New York.

Jayne, J. T., Leard, D. C., Shang, X., Davidots, P., Smith, K. A., Kolb, C. E., and Worsnop, D. R. (2000). Development of an Aerosol Mass Spectrometer for

Downloaded By: [University of Maryland] At: 16:40 17 July 2007

Size and Composition Analysis of Submicron Particles, *Aerosol Sci. Technol.* 33(1–2): 49–70.

Kane, D. B., Oktem, B. et al. (2001). Nanoparticle Detection by Aerosol Mass Spectrometry, *Aerosol Sci. Technol.* 34(6): 520–527.

Knutson, E. O. and Whitby, K. T. (1975). Aerosol Classification by Electric Mobility: Apparatus, Theory, and Applications, *J. Aerosol Science* 6(6): 443–451.

Lee, D., Park, K., and Zachariah, M. K. (2005). Determination of the Size Distribution of Polydisperse Nanoparticles with Single-Particle Mass Spectrometry: The Role of Ion Kinetic Energy, *Aerosol Sci. Technol.* 39(2): 162–169.

Lezius, M., Dobosz, S., Normand, D., and Schmidt, M. (1998). Explosion Dynamics of Rare Gas Clusters in Strong Laser Fields, *Phys. Rev. Lett.* 80(2): 261.

Mahadevan, R., Lee, D., Sakurai, H., and Zachariah, M. R. (2002). Measurement of Condensed-Phase Reaction Kinetics in the Aerosol Phase Using Single Particle Mass Spectrometry, *J. Phys. Chem. A* 106(46): 11083–11092.

Milchberg, H. M., McNaught, S. J., and Parra, E. (2001). Plasma Hydrodynamics of the Intense Laser-Cluster Interaction, *Phys. Rev. E: Statistical, Nonlinear, and Soft Matter Physics* 64(5–2): 056402/1-056402/7.

Murray, V. J. (2000). Sampling and Analysis of Individual Particles by Aerosol Mass Spectrometry, *J. Mass Spectrom.* 35(5): 585–595.

Noble, C. A. and Prather, K. A. (2000). Real-Time Single Particle Mass Spectrometry: A Historical Review of a Quarter Century of the Chemical Analysis of Aerosols, *Mass Spectrom. Rev.* 19(4): 248–274.

Park, K., Lee, D., Rai, A., Mukherjee, D., and Zachariah, M. R. (2005). Size-Resolved Kinetic Measurements of Aluminum Nanoparticle Oxidation with Single Particle Mass Spectrometry, *J. Phys. Chem. B* 109(15): 7290–7299.

Parra, E., Alexeev, I., Fan, J., Kiong, Y. K., McNaught, S. J., and Milchberg, H. M. (2003). Hydrodynamic Time Scales for Intense Laser-Heated Clusters, *J. Optical Soc. Amer. B: Optical Physics* 20(1): 118–124.

Rai, A., Park, K., Zhou, L., and Zachariah, M. R. (2006). Understanding the Mechanism of Aluminum Nanoparticle Oxidation, *Combustion Theory and Modeling* 10(5): 843–859.

Reents, W. D. and Ge, Z. (2000). Simultaneous Elemental Composition and Size Distributions of Submicron Particles in Real Time Using Laser Atomization/Ionization Mass Spectrometry, *Aerosol Sci. Technol.* 33(1–2): 122–134.

Salt, K., Noble, C. A., and Prather, K. A. (1996). Aerodynamic Particle Sizing versus Light Scattering Intensity Measurement as Methods for Real-Time Particle Sizing Coupled with Time-of-Flight Mass Spectrometry, *Anal. Chem.* 68(1): 230–234.

Suess, D. T. and Prather, K. A. (1999). Mass Spectrometry of Aerosols, *Chem. Rev.* 99(10): 3007–3036.

Wang, S., Zordan, C. A., and Johnston, M. V. (2006). Chemical Characterization of Individual, Airborne Sub-10-nm Particles and Molecules, *Anal. Chem.* 78(6): 1750–1754.

Zhou, L., Rai, A., and Zachariah, M. R. (2006). Component and Morphology Biases on Quantifying the Composition of Nanoparticles Using Single-Particle Mass Spectrometry. *Intl J. Mass Spectrom.* 258(1–3): 104–112.